

# We are IntechOpen, the world's leading publisher of Open Access books Built by scientists, for scientists

6,900

Open access books available

186,000

International authors and editors

200M

Downloads

Our authors are among the

154

Countries delivered to

TOP 1%

most cited scientists

12.2%

Contributors from top 500 universities



WEB OF SCIENCE™

Selection of our books indexed in the Book Citation Index  
in Web of Science™ Core Collection (BKCI)

Interested in publishing with us?  
Contact [book.department@intechopen.com](mailto:book.department@intechopen.com)

Numbers displayed above are based on latest data collected.  
For more information visit [www.intechopen.com](http://www.intechopen.com)



---

# Optical, Mechanical, and Electrical Properties of Polymer Composites Doped by Multiwalled Carbon Nanotubes

---

Gülşen Akin Evingür and Önder Pekcan

Additional information is available at the end of the chapter

<http://dx.doi.org/10.5772/63054>

---

## Abstract

Three-dimensional networks can be hydrophilic and/or hygroscopic. Optical, mechanical, and electrical properties of these materials encompass many fields of technology. Composites of carbon nanotubes (CNTs) in polymeric materials have attracted considerable attention in the research and industrial communities due to their unique optical, mechanical, and electrical properties. CNT polymer nanocomposites possess high stiffness, high strength, and good electrical conductivity at relatively low concentrations of CNT filler. Here, in this chapter, we survey the optical, mechanical, and electrical mechanisms for various polymeric systems. Composite gels and films were prepared with various molar percentages of multiwalled carbon nanotubes (MWCNTs). The optical, mechanical, and electrical behaviors of various composite gels doped by MWCNT are also discussed in the each sections of the chapter. The optical behaviors of the composites were performed by the UV-Vis spectroscopy and fluorescence spectroscopy in the first part of the chapter. On the other hand, compressive testing technique and rheological measurements were employed to determine the variations of mechanical properties of the composites in the second part of the chapter. Lastly, we review the electrical properties of the composites improved significantly by addition of MWCNTs researches.

**Keywords:** multiwalled carbon nanotubes (MWCNTs), drying, swelling, elasticity, conductivity, polyacrylamide (PAAm), polystyrene (PS), poly(vinyl acetate-co-butyl acrylate (P(VAc-co-BuA)), latex, PET(poly(ethylene terephthalate)

---

## 1. Introduction

Polymer-carbon nanotube (CNT), discovered by Iijima [1], composites were studied by Ajayan firstly. Carbon nanotubes and their composites have many application areas such as batteries,

flat panel screens, sensors, and nanoprobe [2]. When comparing with different materials, nanotubes are stronger and more conductive than others. Therefore, there are many studies on polymer-CNT composites at last decade [3]. Nanotubes can be described as long and slender fullerenes, in which the walls of the tubes are hexagonal carbon (graphite structure). These tubes can either be single-walled carbon nanotube (SWCNT) or multiwalled carbon nanotube (MWCNT).

N-vinylcarbazole (NVC) was polymerized in bulk or in toluene in the presence of MWCNT without any extraneous catalyst [4]. A composite of PNVC with MWCNT isolated from the polymerization system showed high dc conductivity varying from 1.3 to 33 S cm<sup>-1</sup> depending upon the extent of MWCNT loading in the composite. In situ polymerization and photo-physical properties of poly(p-phenylene benzobisoxazole) (PBO)/MWCNT composites were performed by optical techniques such as UV-Vis absorption, photoluminescence [5]. The investigation of UV-Vis absorption and fluorescence emission spectra exhibited that in situ PBO-MWCNT composite had a stronger absorbance and obvious trend of red-shift compared with blend PBO/MWCNT composites for all compositions. The characterization of poly(3-octylthiophene) (P3OT)/polystyrene (PS)-MWCNT polymer hybrid system performed by Fourier transform infrared spectroscopy, ultraviolet (UV)-visible absorption, and electrical measurements shows significant effects [6]. This study presents that the incorporation of 5 wt % functionalized MWCNT onto P3OT/PS polymer hybrid blend will convert this material from insulator to conductor. Modulation of single-walled carbon nanotubes photoluminescence by hydrogel swelling demonstrated that the shift of nanotubes photoluminescence occurred in a hydrogel matrix. As the hydrogel cross-linking density and hydration state is changed, the nanotubes experience lattice deformations and a shift in photoluminescence emission maxima [7]. CNTs were added into poly(vinyl alcohol) (PVA) hydrogels to modify their mechanical properties. Freezing/thawing method was used for preparing the hydrogels. The tensile modulus, tensile strength, and strain at break of CNT/0.5 specimen with 0.5% (w/w) CNTs are increased by 78.2, 94.3, and 12.7%, respectively, [8]. Dual stimuli responsive poly(N,N-diethylacrylamide-co-acrylic acid) composite hydrogels functionalized with MWCNTs were obtained. Swelling, deswelling, compression properties of the composites were greatly improved [9]. The relaxation process of the composites was modeled by Fickian diffusion mechanism.

Synthesis, electrical, and mechanical properties of polyethylene oxide (PEO)-MWCNT composites were investigated [10]. The conductivity measurements on the PEO-MWCNT composite films with the highest concentration of MWCNT (50 wt%) showed an increase of eight orders 6.52 S cm<sup>-1</sup> of magnitude in conductivity from bare PEO film. The elastic modulus and tensile strength of a PEO-MWCNT film were increased by about fivefold and tenfold, respectively, as compared to the corresponding values for a PEO film.

Polyvinyl alcohol (PVA)-vapor growth carbon fiber (VGCF) and PVA-MWCNT were prepared by gelation/crystallization [11]. The percolation threshold of electrical conductivity for the PVA/MWCNT was <1 wt% MWCNT loading which was much lower than that of PVA/VGCFs composites. The mechanical properties of the PVA composite films were significantly by adding VGCFs and MWCNTs. Poly(ethylene terephthalate)(PET)-MWCNT nanocomposites

were prepared by coagulation method [12]. The percolation threshold 0.6 wt% for rheological property and 0.9 wt% for electrical conductivity has been found. The less rheological percolation threshold than electrical percolation threshold is mainly attributed to the fact that a denser MWCNT network is required for electrical conductivity, while a less dense MWCNT network sufficiently impedes PET chain mobility related to the rheological percolation threshold.

The electrical and rheological characteristics of poly(vinyl acetate) (PVAc)/multiwall carbon nanotube nanocomposites were investigated [13]. Small amount of MWCNT was observed to remarkably decrease resistivity of the nanocomposites. The  $G'$  and  $G''$  increase with the addition of MWCNT loading compared with that of the PVAc matrix.

The rheological and conductivity threshold of semicrystalline syndiotactic polystyrene (sPS) composites filled with CNTs and carbon nanocapules (CNCs) were determined dynamic rheological tests of samples in the melt state and from electrical tests in the solid state, respectively [14]. The sPS composites filled with CNT with a higher aspect ratio exhibited a lower threshold than the CNC filled ones in both rheological and conductivity percolation. The electrical and rheological properties of polypropylene (PP)-CNT composites were studied [15]. Thus, the conductivity of the composites was increased with CNT content and the content percolation threshold is between 1 and 2 wt% MWCNTs.

Poly(N-isopropylacrylamide) (PNIPAAm) containing single-walled carbons and single-walled nanohorns showed phase transitions [16]. Preparation and characterization of PAAm/MWCNTs monohybrid hydrogels with microporous structures were presented by mechanical, pH, and temperature sensitive response and swelling kinetics [17]. The addition of nanotubes produced interesting properties, including tailor ability of temperature responsive swelling and mechanical strength of the PNIPAAm-MWCNT composites. Polystyrene (PS)-MWCNT composites have been widely studied and published in the literature. The results of Yu et al. [18] yield an increment in conductivities of such composites which were produced by latex technology. Poly(vinyl acetate) (PVAc) is a non-crystalline, amorphous thermoplastic polymer. The PVAc is generally fabricated via mixing process with certain polymeric materials in order to reinforce the structural properties [19, 20]. PVAc-based composites are widely used in adhesive, paper, emulsifier, paint, and textile industries due to its high-bond reinforced, film-like, nonflammable, and odorless characteristics [20].

In this chapter, after the introduction section, optical properties of various polymer-CNTs composite will be given and then mechanical properties of them which doped by MWCNTs will be provided. In the later section, electrical properties of them will be discussed.

## 2. Optical properties of different polymer-CNTs composites

Polyacrylamide (PAAm)-MWCNT composite gels were prepared by free radical cross-linking copolymerization [21]. PAAm was doped with various (0.1–15 wt%) of MWCNTs. Before drying was started [22], composites were cut into discs with 10 mm in diameter and 4 mm in

thickness from the injector. Disc-shaped gel samples were placed on the wall of a 1 cm path length, square quartz cell filled with air and water for drying and swelling experiments, respectively.

Drying [22] and swelling [23, 24] process were performed by a Model LS-50 spectrometer of PerkinElmer, equipped with temperature controller. All measurements were made at 90° position, and spectral bandwidths were kept at 5 nm. Pyranine as a fluorescence probe in the composite gels was excited at 340 nm during *in situ* fluorescence experiments, and emission intensities of the pyranine were monitored at 427 nm as a function of drying, and swelling time, respectively. It was observed that the fluorescence intensity of pyranine increased as drying time was increased during the drying process. By combining the Stern-Volmer equation with the moving boundary model, water desorption coefficients,  $D$ , were determined for the drying gels prepared with various MWCNT content at different temperatures.

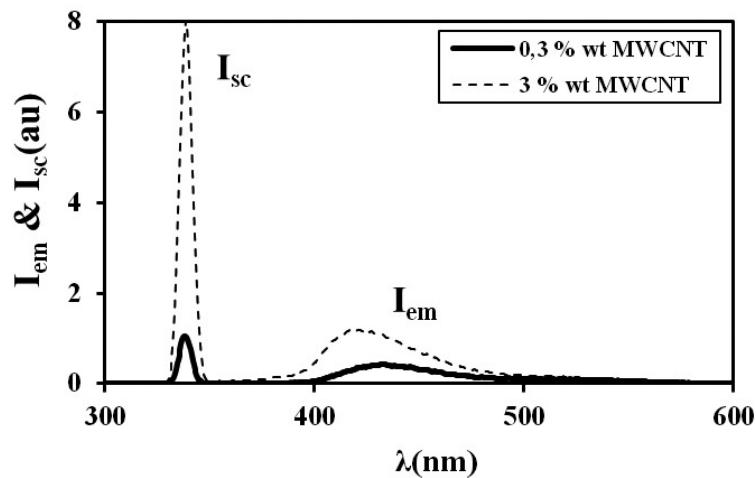


**Figure 1.** Emission spectra of pyranine from composites during drying in air, for 0.3 and 3 wt% MWCNT content gels at 60°C and in 135 min [22].

**Figure 1** shows the emission spectra of pyranine from PAAm-MWCNT composite gel with 0.3 and 3 wt% MWCNT contents during drying in air at 60°C and in 135 min. It can be seen that as the MWCNT content is increased, fluorescence intensity,  $I_{em}$ , decreases relative to the scattered light intensity,  $I_{sc}$ . Since the decrease in  $I_{sc}$  corresponds to the decrease in turbidity of the drying gel [25], the corrected fluorescence intensity,  $I$ , was introduced as  $I_{em}/I_{sc}$  to eliminate the turbidity effect. As far as the correction of fluorescence emission is concern, totally empirical formula was introduced to produce the meaningful results for the fluorescence quenching mechanisms. In order to quantify these results, a collisional type of quenching mechanism may be proposed for the fluorescence intensity,  $I$ , from the gel samples during the drying process using Eq. (1) [26].

$$W = \left(1 - \frac{I}{I_0}\right) \frac{\nu}{k_q \tau_0} \quad (1)$$

$\tau_0$  (=5 ns) is known for pyranine [26] so  $W$  can be calculated using Eq. (1) and the measured  $I$  values, in each drying step.

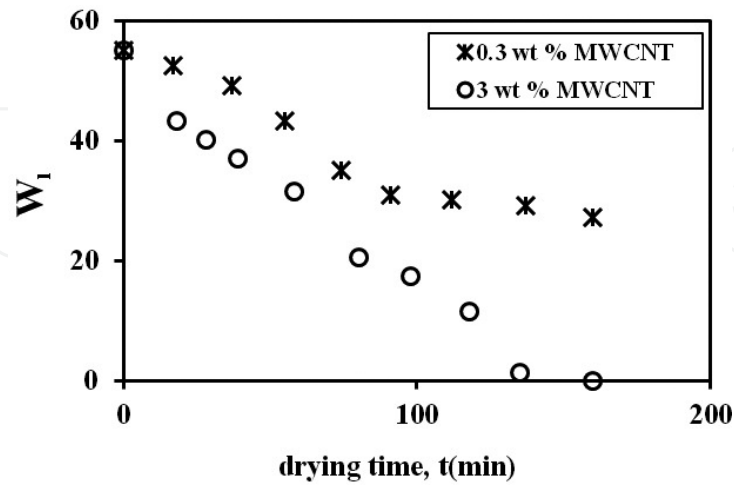


**Figure 2.** The plots of the water release,  $W$  versus drying time,  $t$  for PAAM-MWCNT composite gel dried in air measured by fluorescence technique for 0.3 and 3 wt% MWCNT content samples at 60°C [22].

**Figure 2** presents the  $W_1$  versus drying time. The plots of  $W$  versus  $t^{1/2}$  for 0.3 and 3 wt% MWCNT content sample at 60°C are presented in **Figure 2**, where the fit of the data to Eq. (2) produced the desorption coefficients,  $D_{dl}$  which are plotted in **Figure 3**.

$$\frac{W_l}{W_f} = 2 \left[ \frac{D_{dl}}{\pi a^2} \right]^{1/2} t^{1/2} \quad (2)$$

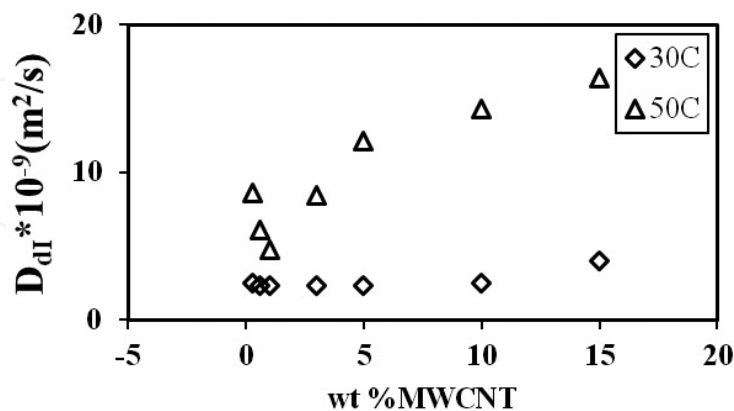


**Figure 3.** Desorption diffusion coefficients,  $D_{dl}$  versus wt% MWCNT content measured by fluorescence technique at 30 and 50°C [23].

Fluorescence technique measures the  $D_{dl}$  values at a molecular level. The desorption coefficients,  $D_{dl}$ , were obtained from Eq. (2) and measured by fluorescence technique for various

MWCNT content samples, where it was observed that the desorption coefficient decreased as the MWCNT content is increased up to 1 wt% MWCNT and reached to a plateau by presenting the different behaviors below and above the critical MWCNT (1 wt%) content at which the conducting percolation cluster starts to appear [21].

Monitoring of swelling experiments shows that emission light intensity,  $I_{em}$ , was decreased which is modeled by the Stern-Volmer equation. The Li-Tanaka equation was used to determine the swelling time constants,  $\tau_s$ , and cooperative diffusion coefficients,  $D_{Sl}$ , from fluorescence intensity (Table 1).

Figure 4 presents the fluorescence spectra of pyranine from the PAAM-MWCNT composite during the swelling process in pure water at 60°C for 1 and 10 wt% MWCNT at 80 min, respectively. When the water uptake is increased, the emission light intensity,  $I_{em}$ , was decreased and the scattered light intensity,  $I_{sc}$ , was increased, respectively, because of the quenching of excited pyranines and turbidity.

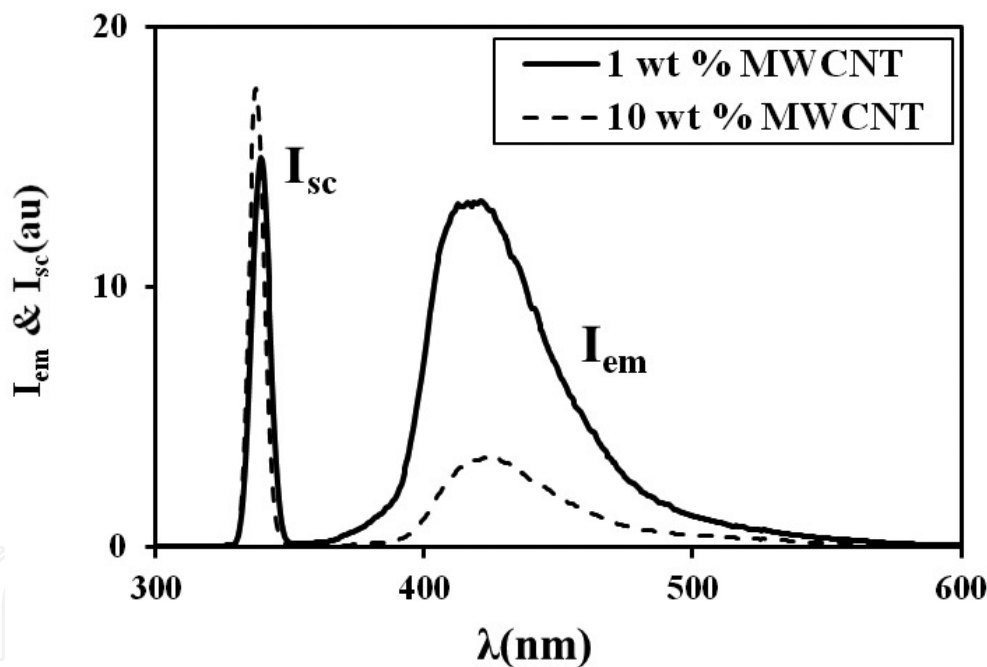
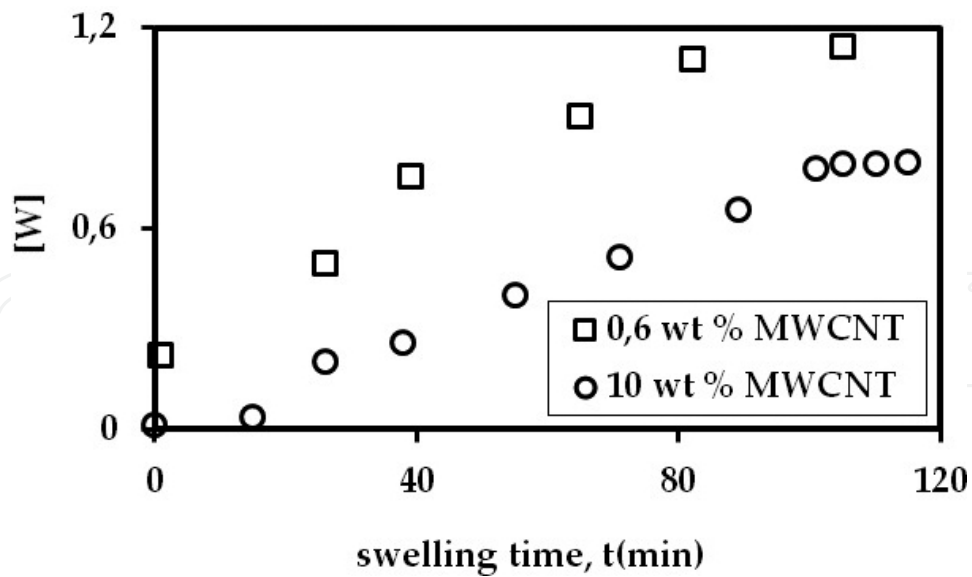


Figure 4. Fluorescence spectra of pyranine from the composite during the swelling process at 60°C for 1 and 10 wt% MWCNT content samples at 80 min [24].

To produce the meaningful results for the fluorescence quenching mechanisms, empirical equation was introduced [27–29]. The corrected fluorescence intensity,  $I$ , is produced by dividing emission light intensity,  $I_{em}$ , to scattering intensity,  $I_{sc}$ , to exclude the effect of turbidity. On the other hand, when quenching of excited pyranines increased, the swelling time,  $t$ , increased. This behavior of the composites was modeled by Stern-Volmer Model have been proposed using Eq. (2) [26].

		$D_{dt} \times 10^{-9} \text{ (m}^2/\text{s)}$	$\tau_s \text{ (min)}$	$D_{st} \times 10^{-9} \text{ (m}^2/\text{s)}$
<b>0</b>	30	14.10	85	0.95
	40	15	48.5	4
	50	26	37.7	7.1
	60	48.67	25	7.3
<b>0.3</b>	30	2.46	58.82	0.6
	40	4.53	55	1.25
	50	8.56	35.71	1.73
	60	9.15	26.31	1.82
<b>0.6</b>	30	2.30	55	0.65
	40	3.17	50	1.7
	50	6.08	33.33	1.9
	60	7.37	25.64	2.5
<b>1</b>	30	2.29	48	1
	40	2.57	47.61	2.07
	50	4.70	32.25	2.44
	60	5.28	22.72	2.95
<b>3</b>	30	2.30	96	0.4
	40	6.23	95.23	0.44
	50	8.39	90.9	0.68
	60	10.2	83.33	0.76
<b>5</b>	30	2.35	98	0.38
	40	8.65	97	0.39
	50	12.1	95.23	0.59
	60	12.7	89	0.62
<b>10</b>	30	2.46	100	0.36
	40	9.88	98	0.37
	50	14.3	95	0.55
	60	14.2	91	0.6
<b>15</b>	30	4	120	0.32
	40	10.4	111.11	0.35
	50	16.4	105.26	0.44
	60	17.6	103.09	0.46

**Table 1.** Experimentally measured parameters of PAAm-MWCNT composites for various temperature and wt% MWCNT contents during drying and swelling processes, respectively.



**Figure 5.** The plots of fluorescence data using Eq. (2) versus swelling time,  $t$ , for PAAm-MWCNT composite gels swollen in water measured by fluorescence technique for 0.6 and 10 wt% MWCNT content sample at 60°C, respectively.

Plots of water uptake,  $W$ , versus swelling time are presented in **Figure 5** for 0.6 and 10 wt% MWCNT content samples at 60°C, respectively. These are typical solvent uptake curves, obeying the Li-Tanaka equation is Eq. (3) [27–29].

$$\frac{W}{W_f} = 1 - B_1 \exp(-t / \tau_s) \quad (3)$$

The logarithmic form of the data was fitted to the following relation produced from Eq. (3)

$$\ln\left(1 - \frac{W}{W_f}\right) = \ln B_1 - \frac{t}{\tau_s} \quad (4)$$

where  $\tau_s$  is the time constant which was calculated from linear regression of the curves in **Figure 5** and Eq. (4) described by Li and Tanaka [28].

$$D_{SI} = \frac{3a_f^2}{\tau_s \alpha_I^2} \quad (5)$$

Using Eq. (5), cooperative diffusion coefficients  $D_{SI}$  were determined for these disc-shaped composites and found to be around  $10^{-9}$  m<sup>2</sup>/s. All  $D_{SI}$  values first increased up to 1 wt% MWCNT content and reached its highest value at this critical point, where the percolation cluster from MWCNT starts to form as given in **Figure 6** and **Table 1**.

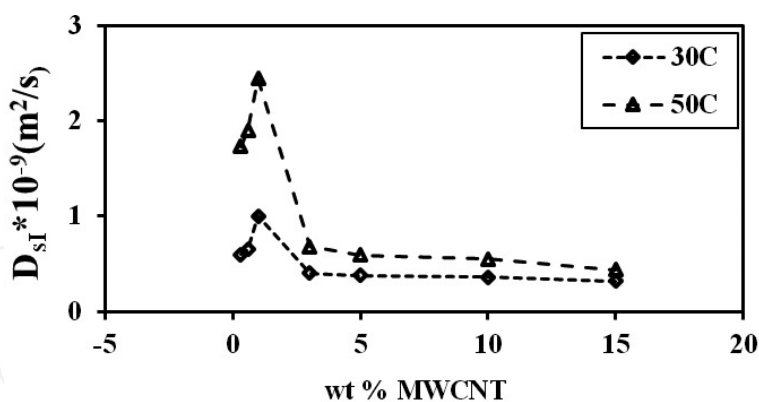


**Figure 6.** Cooperative diffusion coefficient,  $D_{SI}$  versus MWCNT content measured by fluorescence methods at 30 and 50°C, respectively [23].

The percolation cluster formed from CNTs helps water molecules flow faster in their channels and causes the composite gel swell faster presenting large  $D_{SI}$  values for all samples under consideration. However, above the critical point (1 wt% MWCNT), composite gel is quite stiff due to the formation of infinite network from MWCNT. The formation of inelastic composite gel above the critical point then lowers the  $D_{SI}$  values to the smaller numbers.

The results were interpreted in terms of the swelling time constants;  $\tau_s$  (decreased) and the cooperative diffusion coefficient,  $D_{SI}$  (increased) versus wt% MWCNT content. It was observed that high MWCNT content composites swell much slower producing smaller  $D_{SI}$  coefficients for all measurements at a given temperature.

The effect of MWCNT addition in insulating PS matrix was investigated [30]. Composite films were prepared using polystyrene (3.5% w/v) with various (0.13–18 wt%) of MWCNTs stock content on  $2.5 \times 3.0$  cm<sup>2</sup> glass plates at room temperature. Variations in optical properties of very-thin PS-MWCNT composite films were measured using photon transmission techniques. Electrical and optical percolation thresholds were determined. Classical and site percolation theories were used to calculate the critical exponents for optical transmission data.

UV spectrophotometer (Lambda 2 S of PerkinElmer, USA) was used to monitor the variation of optical transparency of the composite films. The transmittances of the composite films were detected at 400 nm wavelength. Measurements were performed at six different positions on the film surface in order to lower the error. All the photon transmission measurements were carried out at room temperature. **Figure 7** shows that the behavior of transmitted ( $I_{tr}$ ) and scattered ( $I_{sc}$ ) light intensities versus the ratio of MWCNT contents ( $M$ ) in composite films. When transmitted light intensity,  $I_{tr}$ , sharply decreases, and scattering centers in the film are increased, respectively, due to refractive indices between two medium in the composite system [30]. In **Figure 7**, the scattered light intensity increases rapidly, even though the MWCNT content was 0.13 wt% at the beginning which shows the percolation threshold value is in between 0 and 0.13 wt%. Since  $M - M_{op} \rightarrow M$  for the extremely low  $M_{op}$  values, the percolation probability for the optical data can be written as follows:

$$I_{sc} = I_0 M^{\beta_{op}} \quad (6)$$

The critical exponent  $\beta_{op}$  was calculated and found to be as 0.32 from the slope of  $\log I_{sc}/I_0$  versus  $\log M$  plot.

The effect of MWCNT addition in insulating PVAc matrix was investigated [31]. Mass fractions of the composites were obtained between 0.5 and 18 wt%. Variations in optical properties of P(VAc-co-BuA)/MWCNT composite films were measured using photon transmission and fluorescence emission measurement techniques. The optical and fluorescence percolation thresholds were determined. The classical and site percolation theories were used to calculate the critical exponents for two data sets from the techniques, respectively.

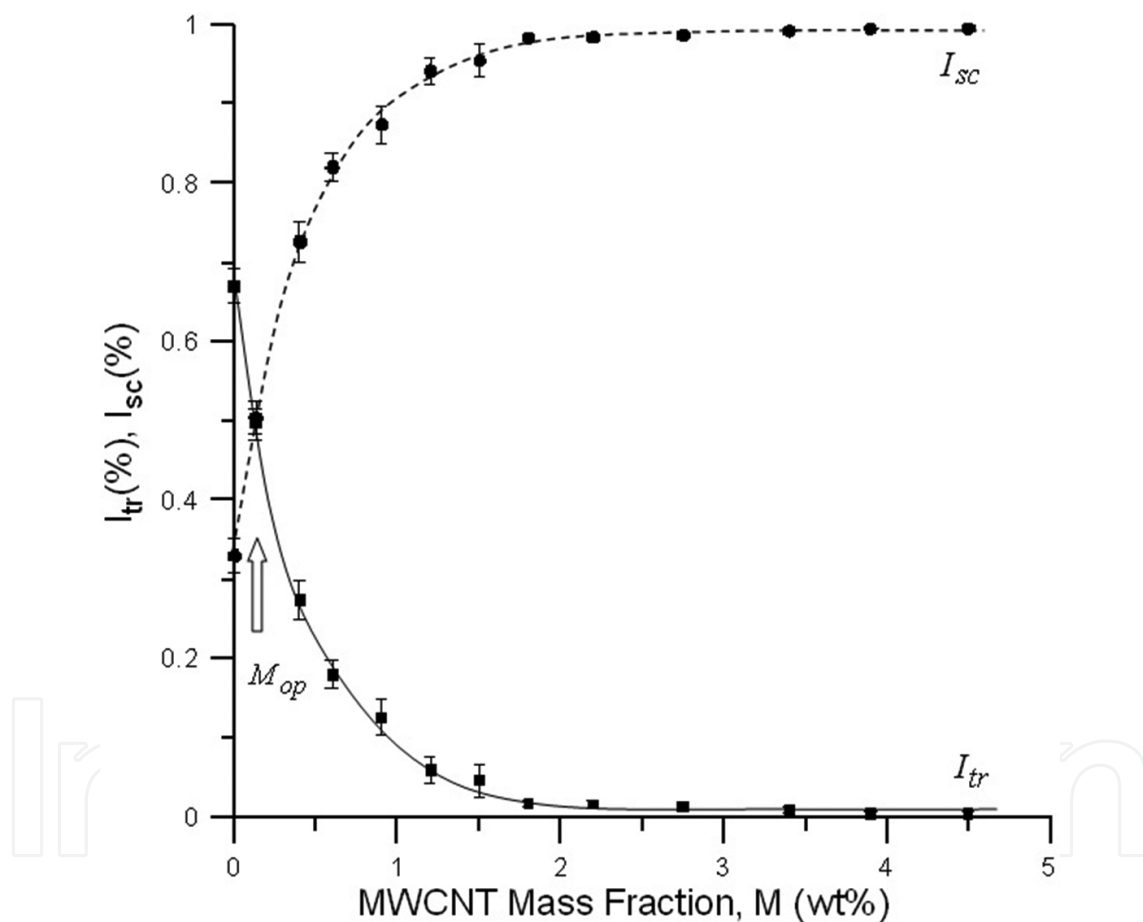


**Figure 7.** Variation in transmitted ( $I_{tr}$ ) and scattered ( $I_{sc}$ ) light intensities on PS-MWCNT composite films versus mass fractions [30].

UV spectrophotometer (Lambda 2S of PerkinElmer, USA) was used to monitor the variation of optical transparency of the composite films. Since the absorbance region of the pyranine molecule was 300–430 nm, the transmittances of the composite films were detected at 470 nm wavelength. Transmission measurements were performed at six different positions on the film surface in order to lower the error. Thus, the average value of transmitted light intensity ( $I_{tr}$ )

was obtained. Transparency variations of the composite films versus mass fractions ( $M$ ) of MWCNT were monitored by transmitted light intensity,  $I_{tr}$ , from the films. It was observed that  $I_{tr}$  sharply decreases as MWCNT content increases in the composite system, and there is almost no light transmission from the films above the mass fraction of 7.0 wt% ( $M \geq 7.0$  wt%).

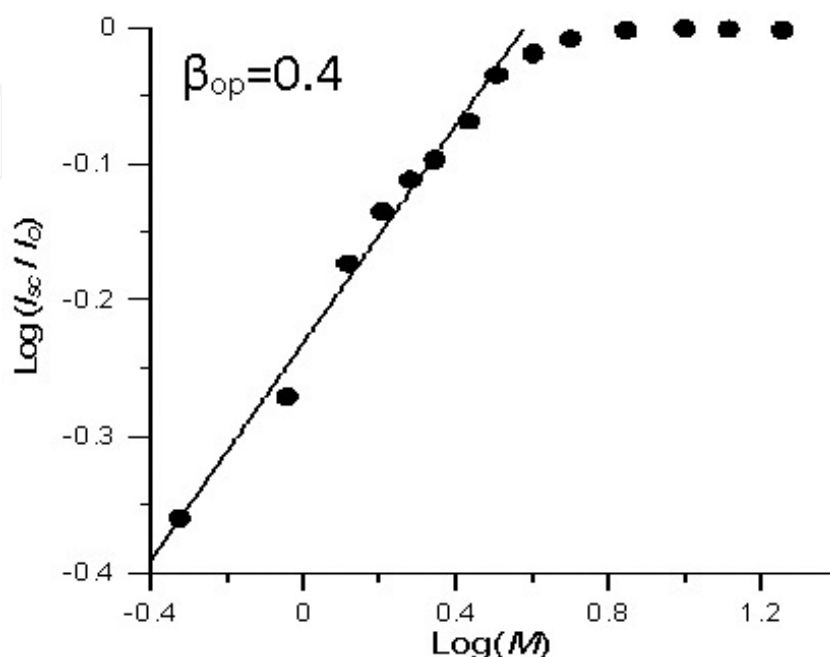


**Figure 8.** The log-log plot of  $I_{sc}$  versus  $M$ . The slope of the straight line produces the optical critical exponent,  $\beta_{op}$ , as 0.40 [31].

The behavior of  $I_{tr}$  versus  $M$  predicts that the composite system owns a percolative structure having a percolation threshold at 0.5 wt% MWCNT content. As  $M$  is increased, the scattered light intensity,  $I_{sc} = I_0 - I_{tr}$ , increases due to the concentration fluctuations.

The variation of  $\log I_{sc}/I_0$  versus  $\log M$  is given in **Figure 8**. The critical exponent,  $\beta_{op}$ , was calculated as 0.40 from the slope of **Figure 8** using Eq. (6). The obtained value of  $\beta_{op} = 0.40$  is not far from the theoretical site percolation value of 0.42 [32].

The variation of fluorescence emission of the composite films was measured using Varian Cary Eclipse fluorescence spectrophotometer. Excitation and emission wavelengths were used as 370 and 507 nm, respectively. The emission wavelength at maximum intensity of pyranine is 510 nm, which varies up to 5–10 nm depending on the structure of the polymer molecules. The fluorescence emission measurements were performed at six different positions on the film surface in order to lower the error level, and the average value of the fluorescence emission intensity ( $I_{fl}$ ) at the maximum was obtained. The maxima of the emission intensity ( $I_{fl}$ ) versus mass fractions ( $M$ ) of the samples are shown in **Figure 9**, where it can be seen that the emission intensities of pyranine show a rapid decrease for further addition of MWCNTs in the composite films. As the MWCNT concentration is increased, the number of the scattering centers in the film also increases.

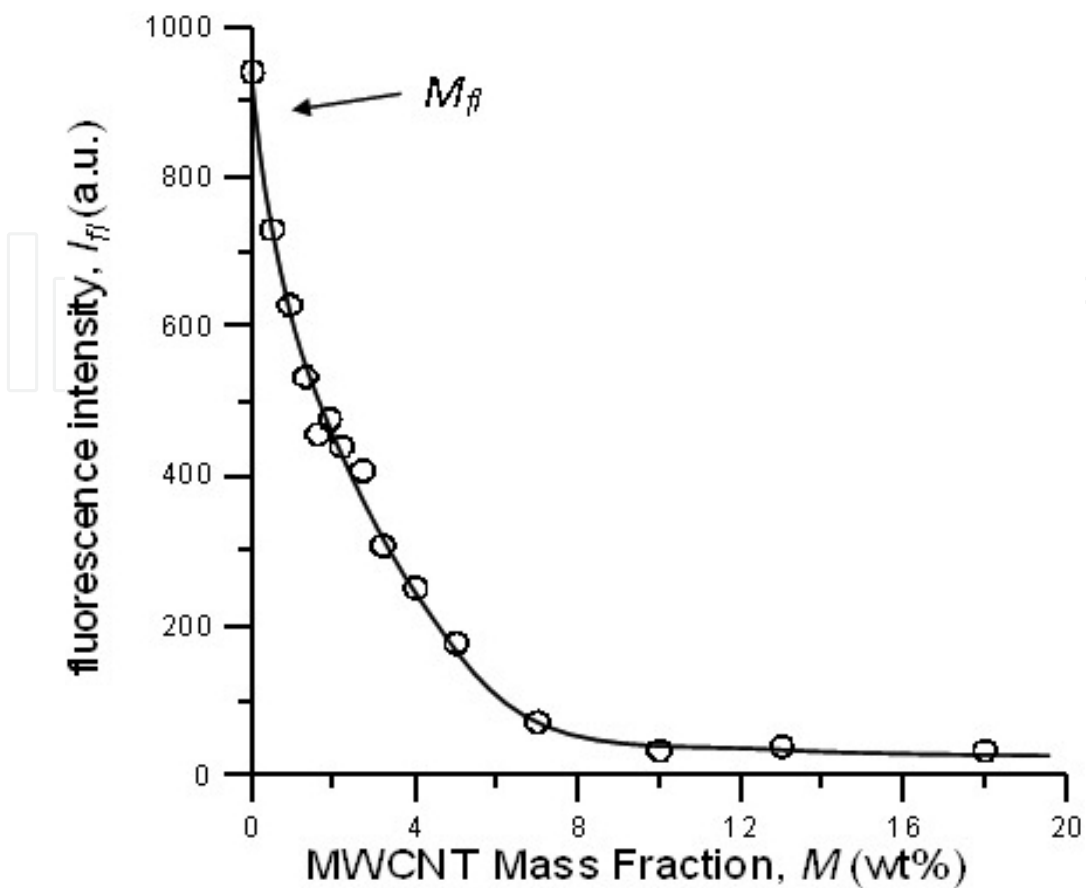


Figure 9. The fluorescence emission intensity,  $I_f$ , versus MWCNT mass fraction,  $M$  [31].

The fluorescence emission data in **Figure 9** can be treated by the percolation theory. The percolation probability for the data of fluorescence emission could be arranged as follows:

$$\frac{1}{I_n} = (M - M_{fl})^{\beta_n} \tag{7}$$

where  $M$  is identical to lattice occupation probability,  $p$ , then the percolation threshold value,  $p_c$ , is equal to  $M_{fl}$ .

Since  $(M - M_{fl}) \rightarrow M$  for low  $M_{fl}$  then Eq. (7) becomes as follows:

$$\frac{1}{I_n} = M^{\beta_n} \tag{8}$$

By assuming, the percolation probability  $P_\infty(p)$  is inversely proportional to the fluorescence emission intensity. The variation of  $\log(1/I_n) - \log(M)$  is presented in **Figure 10**, where two different percolation regions can be detected.

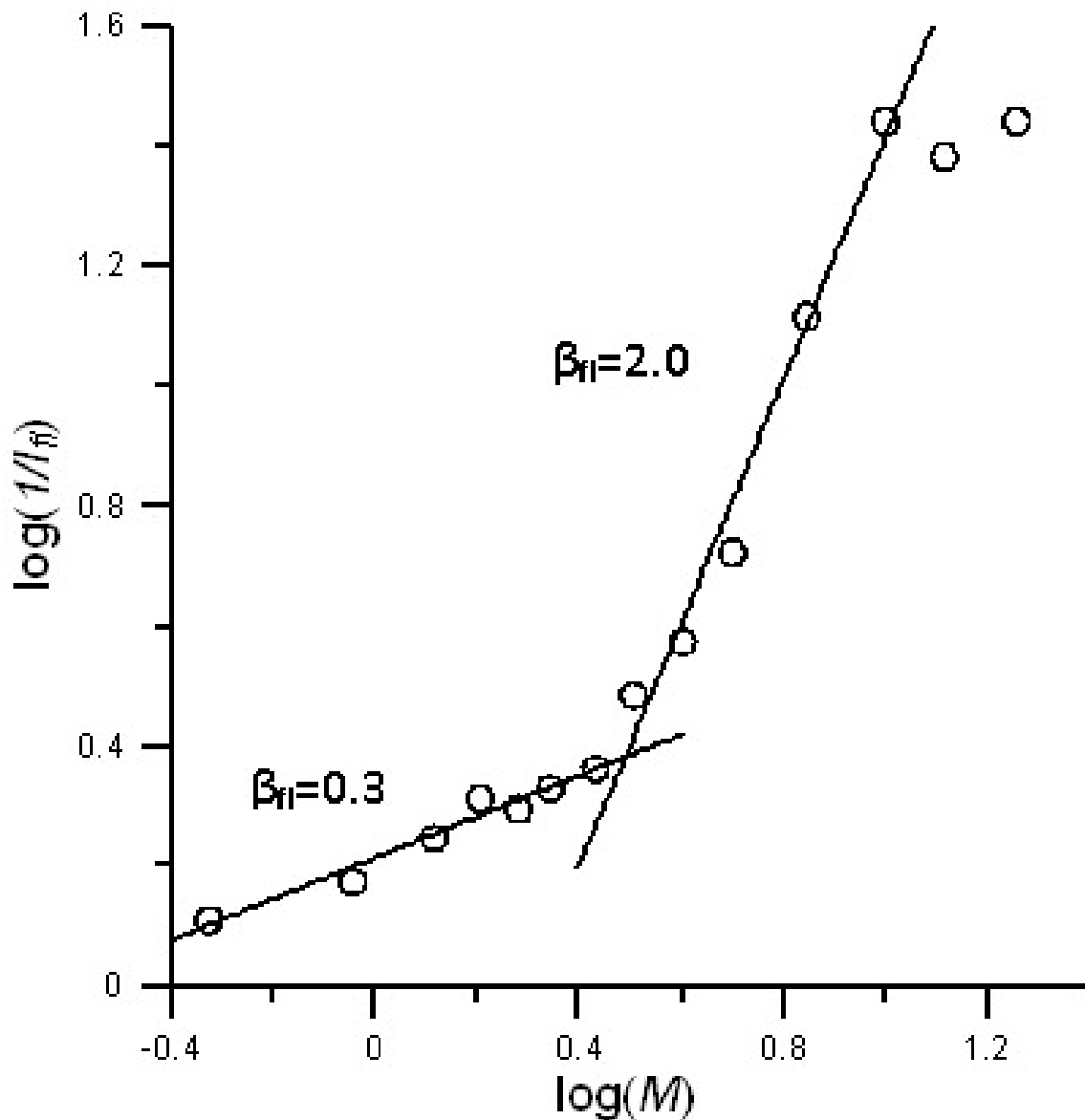


**Figure 10.** The log-log plot of  $1/I_f$  versus  $M$ . The slopes of the straight lines produce the fluorescence critical exponents,  $\beta_{fl}$ , as 0.35 and 2.0 for the low and high MWCNT concentration regions, respectively [31].

The critical exponents,  $\beta_{fl}$ , was calculated and found to be as 0.35 and 2.0 from the slopes of the straight lines in **Figure 10**, according to Eq. (8).

At low MWCNT content, pyranine simply probes the scattering sites in the composite film; however, at high MWCNT concentration, pyranine now traces the conducting network [31].

Polystyrene-MWCNT composite was prepared by Ugur et al. showed that healing and inter diffusion process using photon transmission techniques. After annealing step, the transmitted light intensity,  $I_{tr}$  was monitored to observe the film formation process as shown in **Figure 11**. The increase in  $I_{tr}$  up to healing temperature,  $T_{lv}$  and above  $T_h$  during annealing was explained by void closure and inters diffusion processes, respectively, [33].

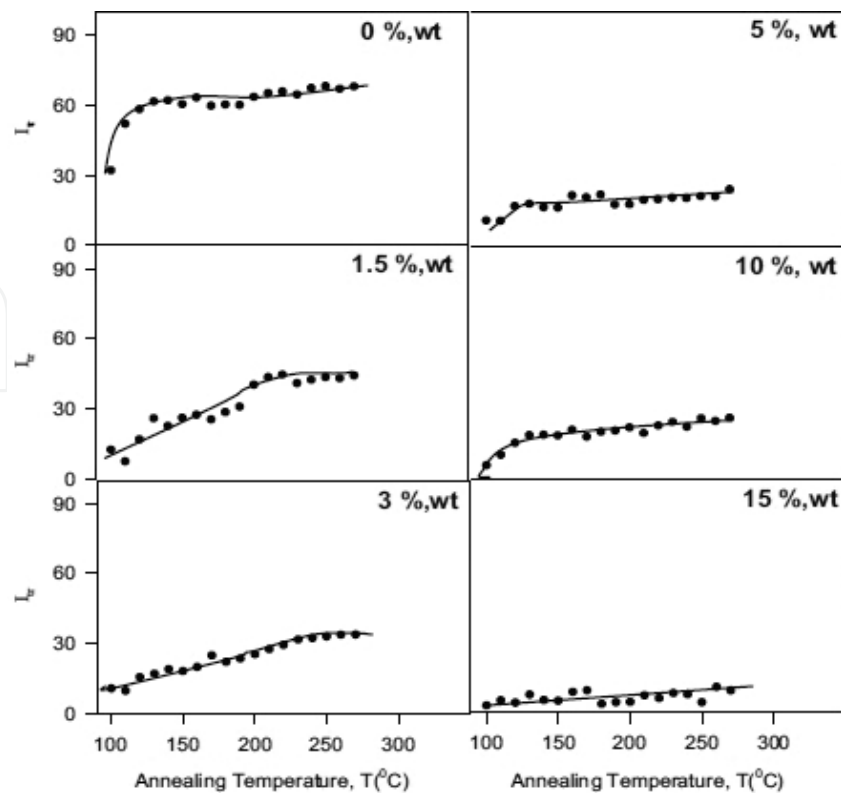


**Figure 11.** Transmitted photon intensities,  $I_{tr}$ , versus annealing temperatures depending on MWCNTs content in the films. Numbers on each figure shows the MWCNTs content [33].

Temperature dependence of oxygen diffusion into polymer-MWCNT composite films was examined by fluorescence spectroscopy [34]. The diffusivity of the composite films was determined by performing oxygen ( $O_2$ ) diffusion measurements within a temperature range of 24–70°C for each film, and pyrene(P) was used as a fluorescence probe (**Figure 12**).

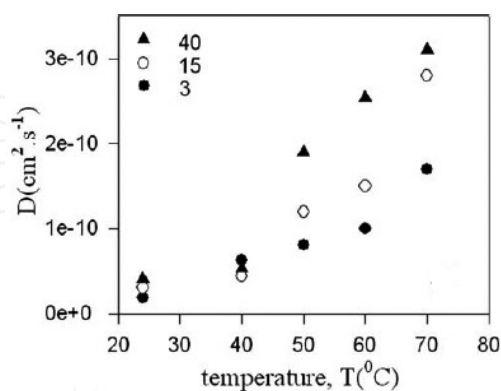


**Figure 12.** Plot of the diffusion coefficients,  $D$ , versus temperatures,  $T$ , for the 3, 15, and 40 wt% MWCNT content films [34].

The diffusion coefficients increased drastically with both increases of MWCNT content and also of the temperature, and this increase was explained via the existence of large amounts of

pores in composite films which facilitate oxygen penetration into the structure. Therefore, PS/MWCNT nanocomposites have useful properties as fluorescent oxygen sensors, and a simple SSF technique can be used to measure the diffusion coefficient of oxygen molecules into these films quite accurately [34]. PS/MWCNT films were prepared by various contents of MWCNT at room temperature. After annealing at 170°C which is above glass transition ( $T_g$ ) temperature of PS, fluorescence quenching processes were realized on oxygen diffusion [35]. **Figure 13** illustrates the logarithmic plots of the fluorescence intensity of pyrene behavior within time during oxygen diffusion into the composite films for 15 wt %MWCNT content.

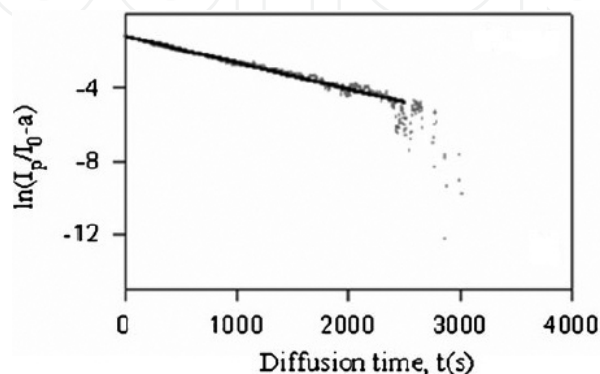


**Figure 13.** Logarithmic plots of the fluorescence intensity of pyrene behavior within time during oxygen diffusion into the composite films for 15 wt %MWCNT content [35].

The diffusion coefficients increased drastically with the increase of MWCNT content, and this increase was explained via the existence of large amounts of pores in composite films which facilitate oxygen penetration into the structure.

Oxygen permeability of nanocomposite films consisting of MWCNT and PS were determined to investigate the oxygen diffusion depending on MWCNT and temperature [36].

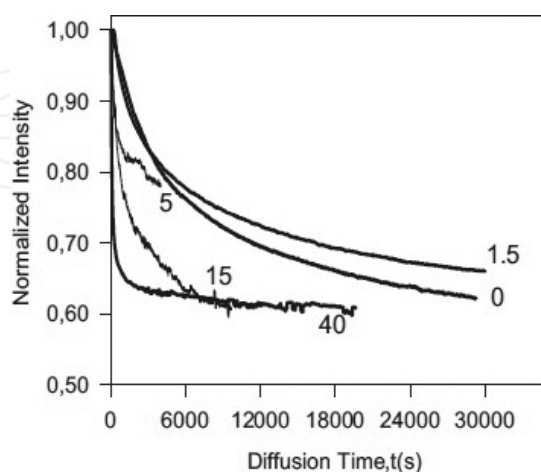


**Figure 14.** The time behavior of pyrene, fluorescence intensity,  $I$ , during oxygen diffusion into the composite films with different MWCNT content. Numbers on each curve indicates the MWCNT content (%) in the film [36].

In **Figure 14** normalized pyrene intensity,  $I_p$  curves are presented against diffusion time for films having different MWCNT content exposed to oxygen. It is seen that as oxygen diffused through the planar film, the emission intensity,  $I_{em}$ , of the pyrene decreased for each MWCNT content film. After completing oxygen diffusion,  $I_{em}$  was saturated. As shown in **Figure 14**, the quenching rate depends on the MWCNT contents in the film. Rapid quenching of excited pyrenes by  $O_2$  molecules is possible for the high MWCNT content composite films [36].

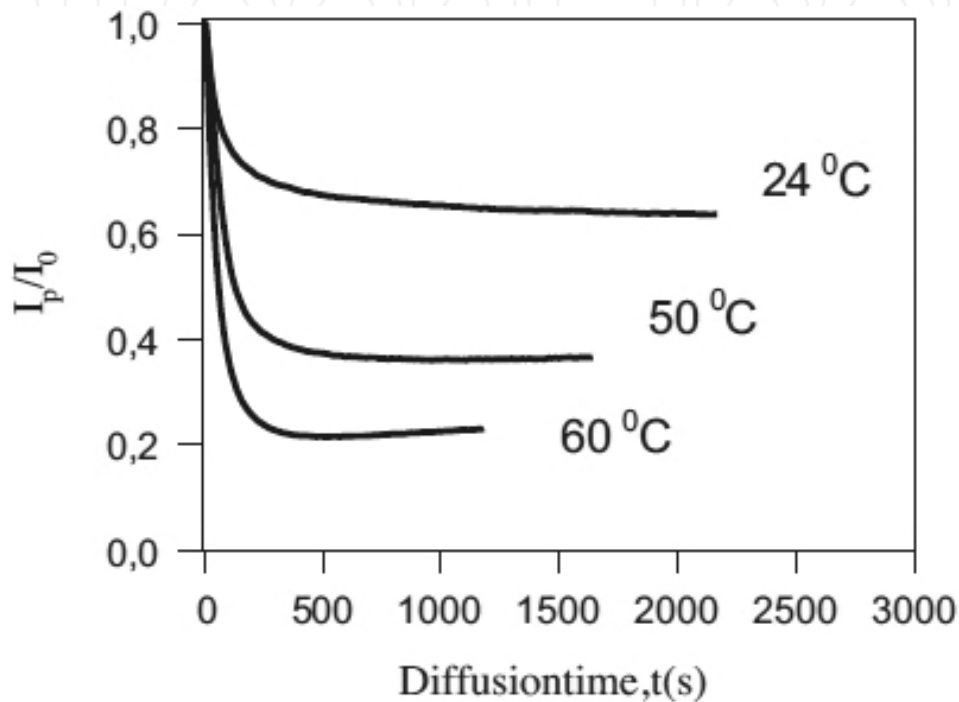


**Figure 15.** The time behavior of the pyrene, P, fluorescence intensity,  $I$ , during oxygen diffusion into the 40 wt% MWCNT content film at various temperatures. Numbers on each curve indicate the temperature [36].

The rate of decrease in intensity is higher at higher temperatures predicting the more rapid quenching of excited pyrene molecules by  $O_2$  molecules diffused into the films. It is worthy to note that in **Figure 15** as expected the  $D$  increases with increase in temperature for all composite films. Increase in temperature naturally increases the Brownian motion of oxygen molecules given them more chance to meet the P molecules in the composite film [36].

The results of **Figures 14** and **15** showed that the diffusion of oxygen was accelerated by both increase in MWCNT fraction and temperature.

PS-MWCNT latex composite films were prepared by mixing of pyrene (P)-labeled PS latex with different amounts of MWCNTs varying in the range between 0 and 20 wt% [37]. To monitor the stages of film formation of PS/MWCNT latex composite films, scattered light ( $I_s$ ) and fluorescence intensities ( $I_p$ ) from P were performed after each annealing step. Some temperatures such as minimum film formation ( $T_o$ ), void closure ( $T_v$ ), and healing, ( $T_h$ ) temperatures were decided as given in **Figure 16**.

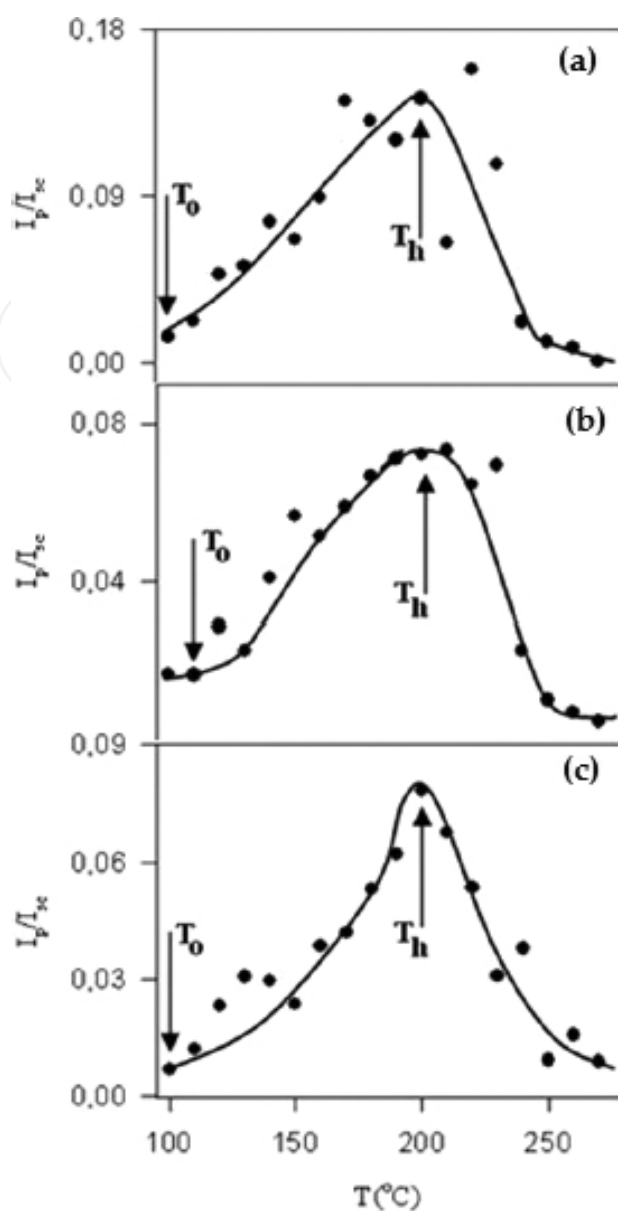


**Figure 16.** Plot of corrected fluorescence intensity (=fluorescence intensity/scattered fluorescence intensity) of composite films with different MWCNT content versus annealing temperatures. (a) 0, (b) 1.5, (c) 3% MWCNT content, respectively [37]. ( $T_0$ , minimum film formation temperature;  $T_h$ , healing temperature).

The existence of MWCNT delays the latex film formation process because of the behavior of  $T_0$ . However, healing processes are not affected by the presence of MWCNT [37].

### 3. The mechanical properties of polymer-CNTs composites

The elastic modulus of the swollen PAAm-MWCNT composites was measured to determine the effect of MWCNTs content. Elasticity measurement was performed by compressive testing technique and modeled by the theory of rubber elasticity [38, 39].

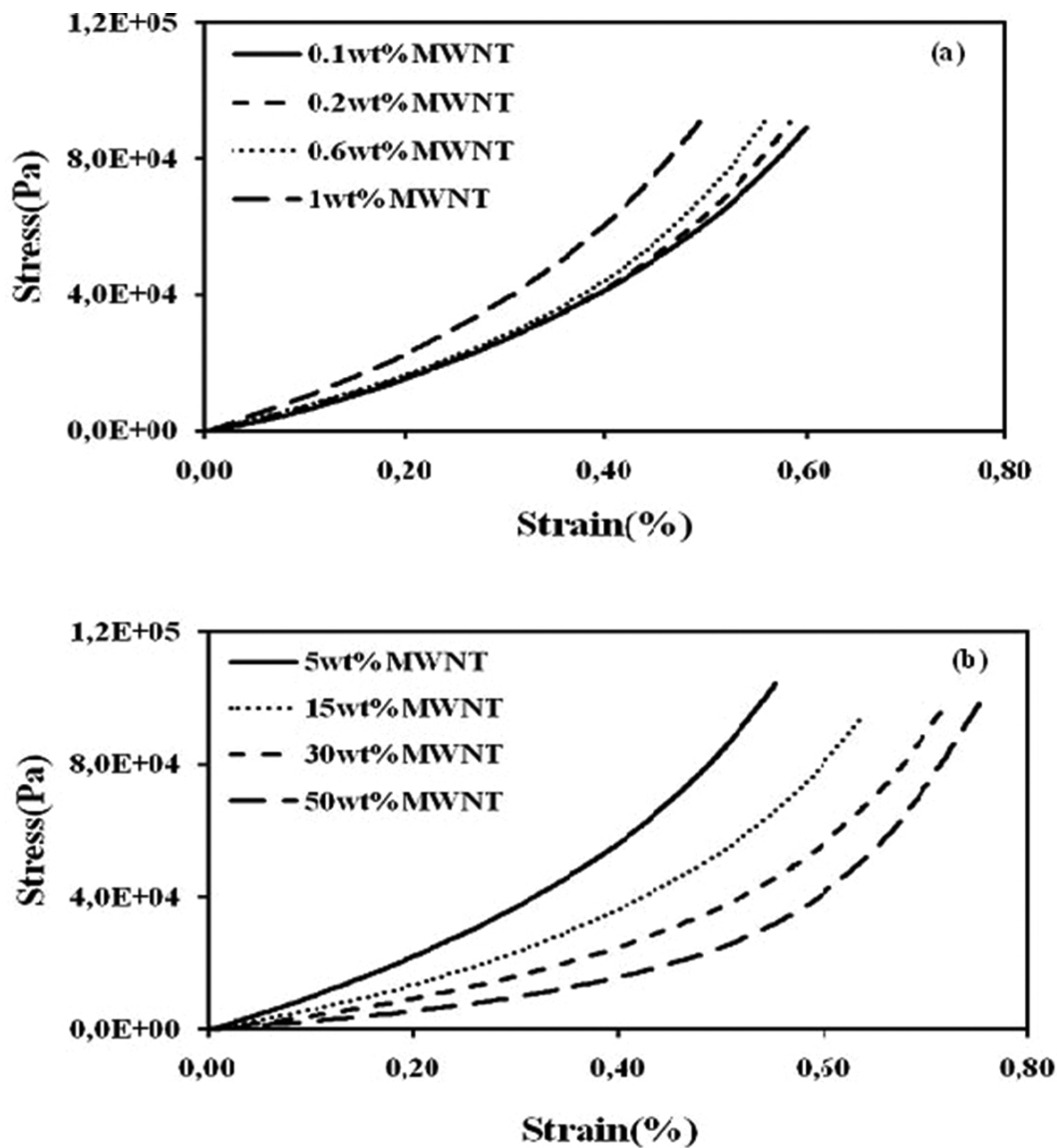


Figure 17. Stress versus strain curves (a) lower and (b) higher MWCNT contents at 25°C, respectively [39].

Stress (Pa)-strain plots of low and high MWCNTs content gels produced using the data obtained from the linear region, in the plots of  $F$  (N) versus compression curves for PAAM-MWCNT composites at 25°C, are presented in Figure 17, respectively. The stress versus strain displays a good linear relationship at 25°C, which agrees with Eq. (9).

$$\tau = G\lambda \quad (9)$$

The elastic moduli were obtained by a least square fit to the linear region of Figure 17. The addition of MWCNT into PAAM caused an increase in elastic modulus of the composite as expected. In PAAM-1 wt% MWCNT composite, the measured elastic modulus is found to be 0.105 MPa, two times larger than pure PAAM sample. It is seen in Figure 17a that PAAM-0.1

wt% MWCNT composite has smaller initial slope than 1 wt% MWCNT content composite. In this case, it appears that the alignment effect of MWCNT plays an important role for getting the different onset behavior [40]. The stress of the PAAm-MWCNT (1–5 wt% MWCNT composites) increases dramatically when the strain exceeds 0.6%, where the alignment is taking place in the composite. On the other hand, at high MWCNT region, the random motion of MWCNT impedes alignment as predicted in **Figure 17b**. Therefore, in a gel with low MWCNT content, alignment of MWCNTs with each other is much easier than in high content MWCNT composite.

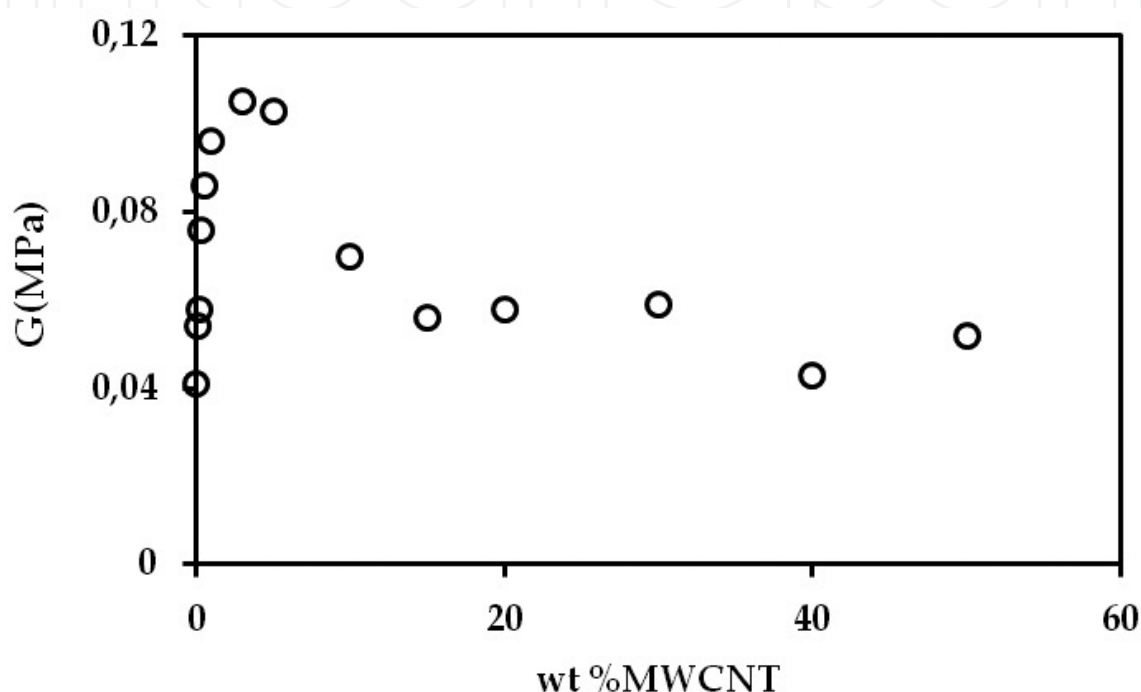


**Figure 18.** Dependence of elastic modulus on content of wt% MWCNT in the composite [39].

**Figure 18** shows the plot of elastic modulus,  $G$  versus MWCNTs content in the composite gel. Elastic modulus increases dramatically up to 1 wt% MWCNT with increasing nanotube content and decreases presenting a critical MWCNT value indicating that there is a sudden change in the material elasticity. The sudden change in  $G$  predicts that the composites have reached a super-elastic percolation network [41]. At contents above 1 wt% MWCNTs, the elastic modulus is decreased marginally with increasing MWCNTs content. On the other hand, at low MWCNT content ( $\leq 1$  wt%), the elastic modulus increases up to 0.105 MPa, only exceeding it when the MWCNT content is above 1 wt%, and then decreases further as the MWCNTs content is raised. At the percolation threshold, 1 wt% the nanotubes form an interconnecting structure, call percolation cluster exhibiting a high degree of nanotube interactions and/or entanglement [42]. The increasing MWCNT content produces infinite network in reducing the swelling and decreasing elastic modulus as was expected for the composites at high MWCNT content. The decrease in elastic modulus,  $G$ , can be explained by the formation of a carbon nanotube network which significantly improves the stiffness of

composite gel. That is due to the high stiffness the mechanical properties should be influenced substantially [43]. On the other hand, when the MWCNT content is below 1 wt%, the elastic modulus is presenting lower values and increases as MWCNT is added. Because of molecular tube-tube and tube-polymer interactions, the mechanical properties of MWCNT-polymer composites were affected. On the other hand, to determine mechanical properties of MWCNT-polymer composites, load transfer and interfacial bonding should be known. Therefore, nanotube dispersion in the polymer plays a critical role for this phenomenon [40].

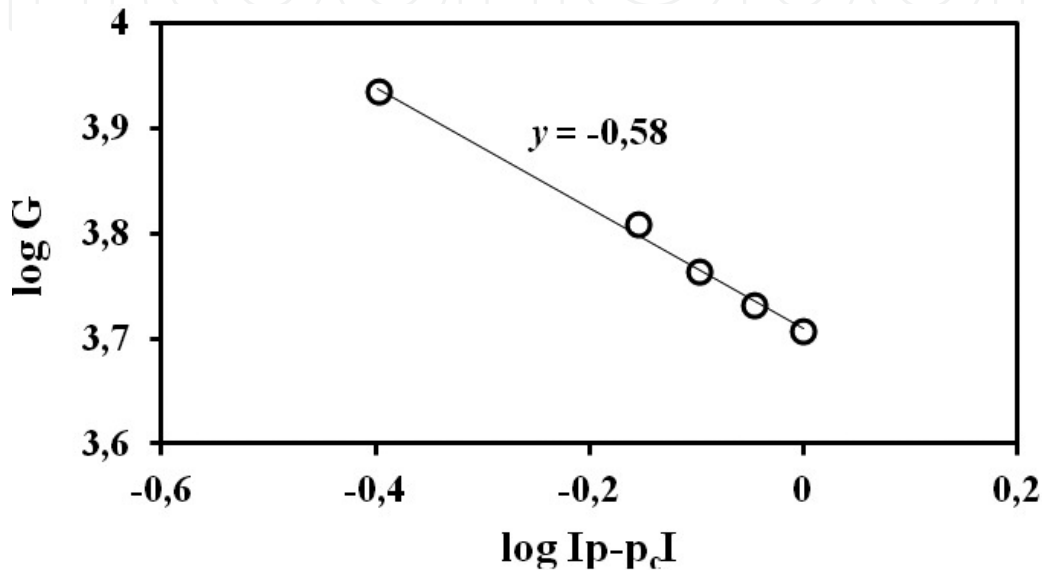


**Figure 19.** Logarithmic plot of the elastic modulus versus MWCNTs contents curves for  $p < p_c$ . The exponent,  $y$ , was determined from the slope of the straight line [39].

In **Figure 19**, it is understood that 1 wt% is the critical percolation threshold,  $p_c$ , at which gel system owns a percolation cluster formed from MWCNTs. Here, the composite gel passes the highest elasticity presenting the highest  $G$  value.

$$G(p) \approx (p_c - p)^{-y} \quad (10)$$

Equation (10) now can be used to fit the  $G$  versus wt% MWCNT curve below the critical point (below 1 wt%). The value of the fitting exponent  $y$  in Eq. (10) was estimated from the slope of the linear relation between  $\log G$  and  $\log Ip-p_cI$ , as shown in **Figure 19**. Elastic percolation occurs below 1 wt% MWCNTs (**Figure 18**) with a critical exponent around  $y = 0.58$ , which is close to the theoretical prediction of this value in the 3D percolated system known as a SEP. The critical exponent,  $y$ , agrees with the literature values [44]. Here,  $x$  is the critical exponent which is taken from literature by the upper limit  $x = 2.1$ . Moreover,  $\Delta$  was found to be 0.74, very close to the upper limit of  $\Delta$ , as given in range between 0.61 and 0.75. The mechanical properties of PVAc-MWCNT nanocomposites [13] were investigated as shown in **Figure 20**.

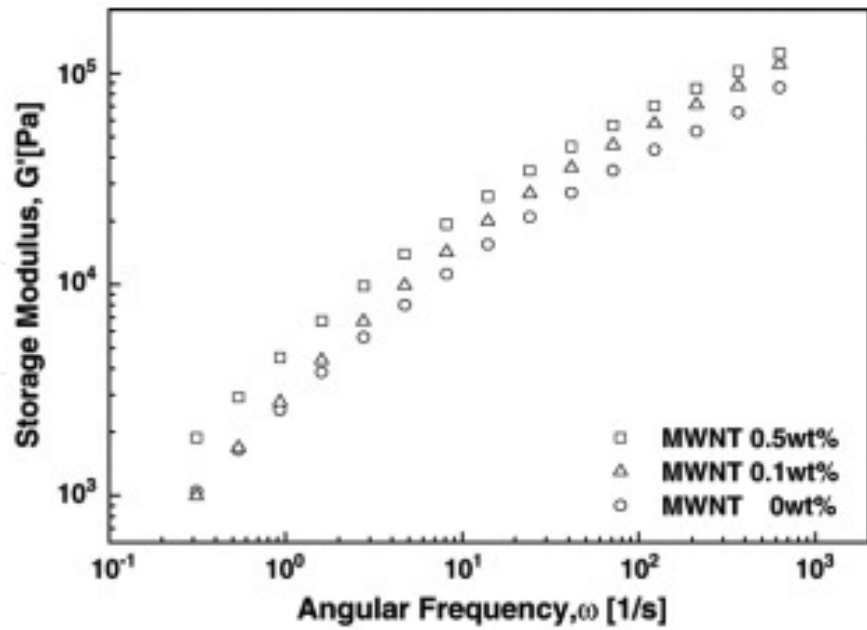


Figure 20. Storage modulus as a function of angular frequency at 145°C for PVAc-MWCNTs nanocomposites [13].

As shown in Figure 20, the storage modulus  $G'$  increases with an addition of MWCNT loading compared with that of the PVAc matrix.

The rheological properties of PET-MWCNT nanocomposites were determined using low strain values with frequency 0.1–500 rad/s [46]. The storage modulus versus frequency is given in Figure 21.

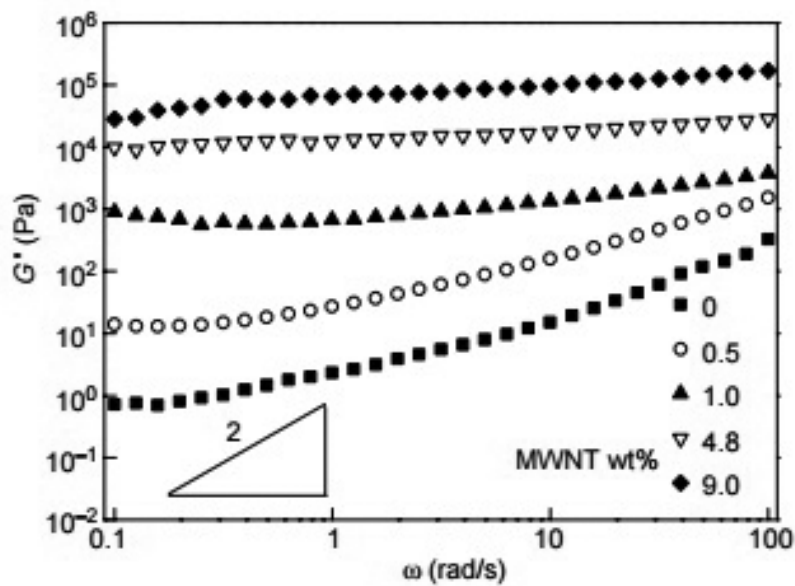


Figure 21. Storage modulus ( $G'$ ) of PET-MWCNT nanocomposites versus frequency ( $\omega$ ) at 265°C [12].

The rheological behavior of the nanocomposites depends on the MWCNT content with respect to the frequencies because of the restriction of PET chain relaxation and the short-range dynamics or local motion of the PET chains in the nanocomposites [12].

#### 4. The electrical properties of polymer-CNTs composites

The electrical resistivity of the PVAc/MWCNT composite films was performed by a Keithley Model 6517A electrometer and Keithley Model 8009 resistivity test fixture. 10–100 V DC potential for every 15 s periods was applied to measure their surface resistivity,  $R_s$  (Ohm/square or Ohm) which was four different orientations and repeated measurements were repeated. The surface conductivity values were calculated from the following equation.

$$\sigma = 1 / R_s \quad (11)$$

Then, the obtained results from Eq. (11) are presented in **Figure 22**. It can be seen from **Figure 10** that the conductivity,  $\sigma$ , dramatically increases above  $M_\sigma = 1.8$  wt%. This behavior can be explained by the existence of vertical conductive paths of MWCNTs in the composite film. After  $M_\sigma = 1.8$  wt%, the insulating system starts to transform to the conductive system. Therefore,  $M_\sigma = 1.8$  wt% is the percolation threshold of conductivity. For a dilute composite structure, classical percolation theory was given in Eq. (12) can be used [25].

$$\sigma = \sigma_0 (M - M_\sigma)^{\beta_\sigma} \quad (12)$$

Here,  $\sigma$  is the conductivity (Siemens),  $\sigma_0$  is the conductivity of pure MWCNT film,  $M$  is the volume or mass fraction of MWCNT,  $M_\sigma$  is the percolation threshold value, and  $\beta_\sigma$  is the critical exponent for the conductivity, respectively, which was calculated from Eq. (12) and determined from the slope of the  $\log \sigma$  and  $\log (M - M_\sigma)$  plot. The  $\beta_\sigma = 2.25$  value is well agreed with the theoretical and the experimental data in the literature [45].

The average values of the surface resistivity,  $R_s$ , of PVAc/MWCNT composite films versus mass fractions of MWCNT,  $M$ , were measured and observed that the surface resistivity ( $R_s$ ) of the composite films do not change much below 1.0 wt% ( $M \leq 1.0$  wt%)[45]. However,  $R_s$  values of the composite films dramatically decrease from  $10^{11}$  to  $10^4$  Ohm/square in the bandgap of  $M = 1.0$ – $4.0$  wt%.

This behavior indicates that the electrical percolation occurs at low levels of  $M$ . The surface conductivity values were calculated from Eq. (11). The percolation threshold of the surface conductivity ( $M_\sigma$ ) is 1.0 wt%.  $\beta_\sigma$  was calculated from the slope of the curve in **Figure 23**, which was drawn from the logarithms of the surface conductivity data treated with Eq. (12), and found to be as 2.1 which is well agreed with the theoretical and the experimental results in the literature [45].

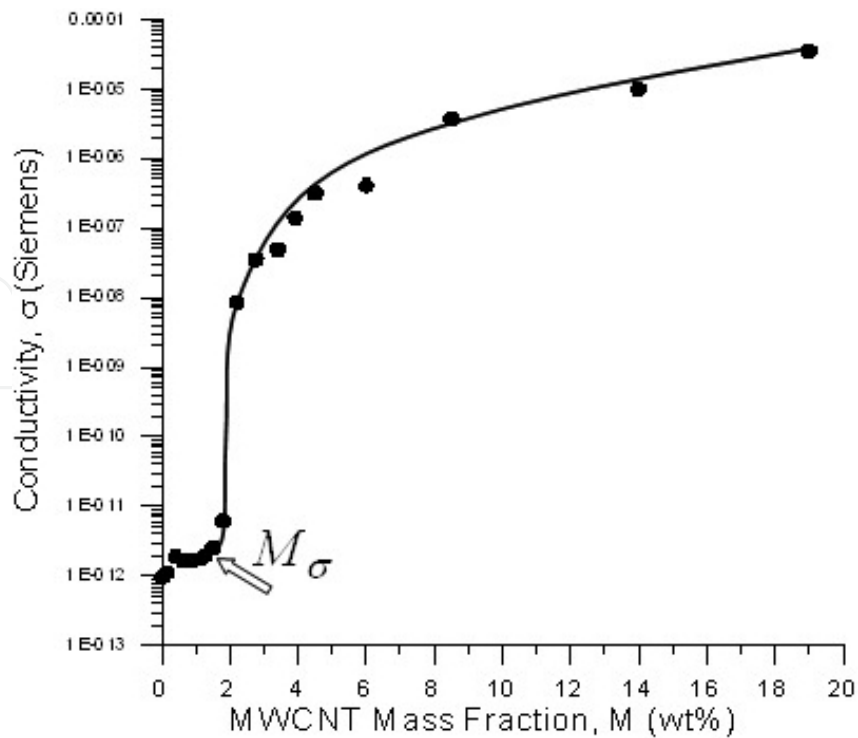


**Figure 22.** Variations in conductivities,  $\sigma$ , which were calculated by Eq. (11) versus mass fractions [30].

The surface conductivity properties of PS-MWCNT composite films were measured at room temperature using a two probe technique [30]. **Figure 24** shows the electrical conductivity ( $\sigma$ ) of PS-MWCNT composite films as a function of MWCNT ratio, R. While low MWCNT content composites ( $R < 0.04$ ) show similar conductivity between  $10^{-13}$  and  $10^{-12}$ , the conductivity of high MWCNT content films ( $R > 0.04$ ) increases dramatically to  $10^{-7}$ – $10^{-6}$  S.

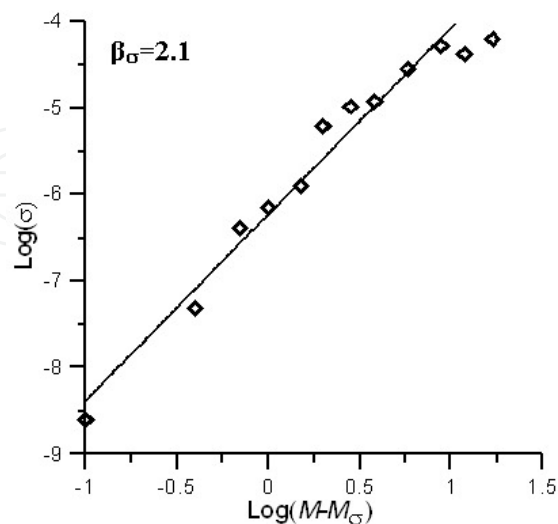


**Figure 23.** The log-log plot of  $\sigma$  versus  $M \rightarrow M_\sigma$ . The slope of the straight line produces the electrical critical exponent,  $\beta_\sigma$  as 2.1 [31].

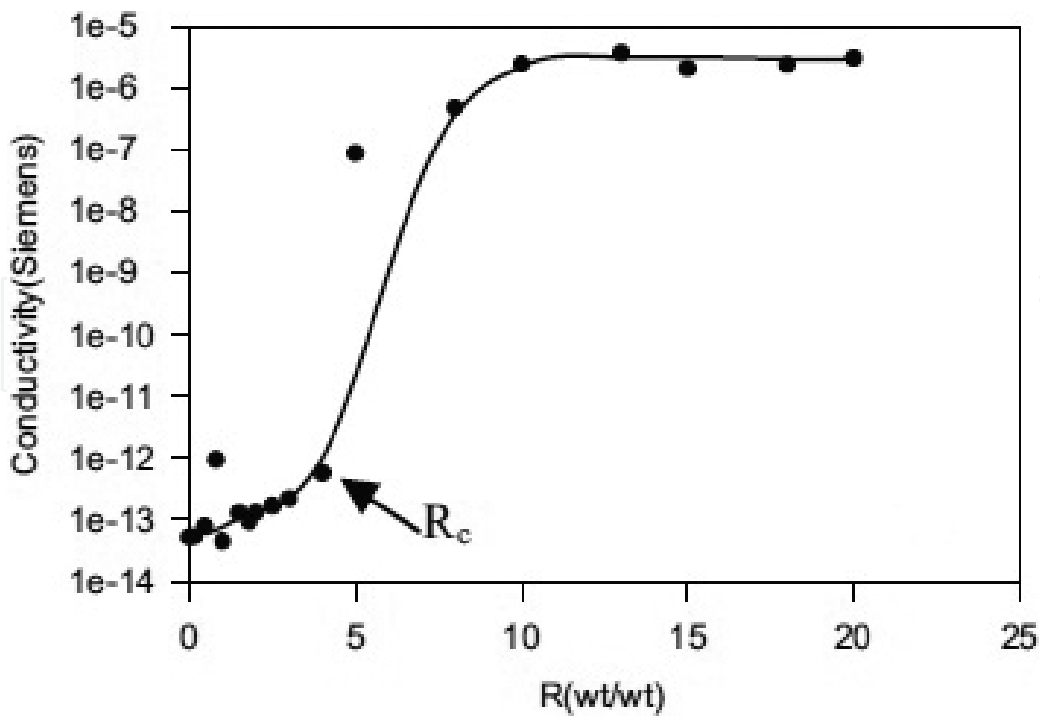


Figure 24. Conductivity versus MWCNT content, R (w/w) [30].

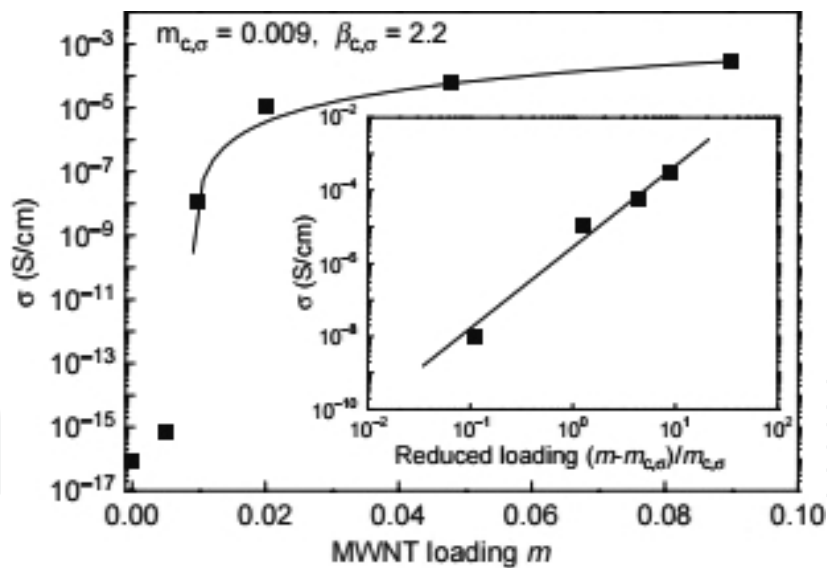


Figure 25. Electrical conductivity ( $\sigma$ ) of the PET-MWCNT nanocomposites as a function of MWCNT loading. Inset: a log-log plot of electrical conductivity versus reduced MWCNT loading. The solid lines are fits to a power law dependence of electrical conductivity on the reduced MWCNT loading [12].

Figure 25 shows the electrical conductivity ( $\sigma$ ) of the PET-MWCNT [12]. The electrical conductivity of pure PET is  $8.6 \times 10^{-17} \text{ S cm}^{-1}$ . By loading MWCNT from 0.5 to 1 wt%, the conductivity of PET-MWCNT nanocomposites increases in 8 orders of magnitude, because percolative path was formed in the nanocomposite [12].

## 5. Conclusion

In this chapter, we review the optical, electrical, and mechanical behaviors of polymers doped by multiwalled carbon nanotubes (MWCNTs). This chapter covered the works produced from different types of polymers. We try to give the experimental results based on the mentioned theoretical models. In the first section of the chapter, some examples were given about optical behavior of polymer-MWCNT composites which were performed by fluorescence and UV-Vis spectroscopy. Therefore, the behavior of them at a molecular level were discussed, and measured some physical quantities were reported. The second section of the chapter has demonstrated that the mechanical and rheological measurements can be used to determine the variations of the elastic and storage modulus of the composites. The third part of the chapter has shown that the insulator-conductor transition takes place by the addition of a small amount of MWCNT in the polymer composite system. The insulator system starts to transform to a more conductive state by consisting of conductive paths of MWCNTs between the electrodes. The size of MWCNTs and electron hopping and/or tunneling effects play important roles in the early percolation behavior of the films.

In conclusion, we try to give the experimental evidences based on the mentioned theoretical models. As far as the engineering applications are concerned, optical, mechanical, and electrical properties of polymer composites prepared by MWCNT contents are very important in coating, food, electronic, and pharmaceutical industries. This chapter introduces basic parameters for the given processes in the polymer composites which can find important applications in the mentioned fields.

## Author details

Gülşen Akın Evingür<sup>1\*</sup> and Önder Pekcan<sup>2</sup>

\*Address all correspondence to: [gulsen.evingur@pirireis.edu.tr](mailto:gulsen.evingur@pirireis.edu.tr)

1 Piri Reis University, Tuzla, İstanbul, Turkey

2 Kadir Has University, Cibali, İstanbul, Turkey

## References

- [1] Lijima, S. Helical microtubules of graphitic carbon. *Nature*. 1991; 354: 56–58.
- [2] Ajayan PM, Zhou OZ. Applications of carbon nanotubes. *Carbon Nanotubes*. 2001; 80: 391–425.

- [3] Olek M. Carbon Nanotube Composites Mechanical, Electrical and Optical Properties. Mathematics and Nature Department, Bonn University, Bonn, Germany. 2006.
- [4] Maity A, Biswas M. Polymerization of N-vinylcarbazole by multiwalled carbon nanotube. *Journal of Applied Polymer Science*. 2007; 104: 4121–4126.
- [5] Zhou C, Qiu X, Zhuang Q, Han Z, Wu Q. In situ polymerization and photophysical properties of poly(p-phenylene benzobisoxazole)/multiwalled carbon nanotubes composites. *Journal of Applied Polymer Science*. 2012; 124: 4740–4746.
- [6] Ibrahim SS, Ayesh AS. Electrical and optical properties of functionalized multiwalled carbon nanotubes/poly(3-octylthiophene)/polystyrene composites. *Journal of Thermo-plastic Composite Materials*. 2015; 28(2): 225–240.
- [7] Barone PW, Yoon H, Garcia RO, Zhang J, Ahn JH, Kim JH, Strano MS. Modulation of single walled carbon nanotube photoluminescence by hydrogel swelling. *ACS Nano*. 2009; 3(12): 3869–3877.
- [8] Tong X, Zheng J, Lu Y, Zhang Z, Cheng H. Swelling and mechanical behaviors of carbon nanotube/poly(vinyl alcohol) hybrid hydrogels. *Materials Letters*. 2007; 61: 1704–1706.
- [9] Liu H, Liu M, Zhang L, Ma L, Chen J, Wang Y. Dual stimuli sensitive composites based on multi walled carbon nanotubes and poly(N,N-diethylacrylamide-co-acrylic acid) hydrogels. *Reactive & Functional Polymers*. 2010; 70: 294–300.
- [10] Awasthi K, Awasthi S, Srivastava A, Kamalakaran R, Talapatra S, Ajayan PM, Srivastava ON. Synthesis and characterization of carbon nanotube-polyethylene oxide composites. *Nanotechnology*. 2006; 17: 5417–5422.
- [11] Bin Y, Mine M, Koganemaru A, Jiang X, Matsuo M. Morphology and mechanical and electrical properties of oriented PVA–VGCF and PVA–MWNT composites. *Polymer*. 2006; 47: 1308–1317.
- [12] Hu G, Zhao C, Zhang S, Yang M, Wang Z. Low percolation thresholds of electrical and rheology in poly(ethylene terephthalate through the networks of multi walled carbon nanotubes). *Polymer*. 2006; 47: 480–488.
- [13] Choi CS, Park BJ, Choi HJ. Electrical and rheological characteristics of poly(vinyl acetate)/multiwalled carbon nanotube nanocomposites. *Diamond Related Materials*. 2007; 16: 1170–1173.
- [14] Huang CL, Wang Chi. Rheological and conductive percolation laws for syndiotactic polystyrene composites filled with carbon nanocapsules and carbon nanotubes. *Carbon*. 2011; 49: 2334–2344.
- [15] Seo MK, Park SJ. Electrical resistivity and reological behaviors carbon nanotubes filled polypropylene composites. *Chemical Physics Letters*. 2005; 395: 44–48.

- [16] Miyako E, Nagata H, Hirano K, Hirotsu T. Photodynamic thermoresponsive nanocarbon-polymer hybrids. *Small* (Weinheim an der Bergstrasse, Germany). 2008; 4(10): 1711–1715.
- [17] Luo YL, Zhang CH, Chen YS, Yang W. Preparation and characterization of polyacrylamide/MWNTs nanohybrid hydrogels with microporous structures. *Materials Research Innovations*. 2009; 13(1): 18–27.
- [18] Yu J, Lu K, Sourty E, Grossiord N, Koning CE, Loos J. Characterization of conductive multiwall carbon nanotube/polystyrene composites prepared by latex technology. *Carbon*. 2007; 45: 2897–2903.
- [19] Choi CS, Park BJ, Choi HJ. Electrical and rheological characteristics of poly(vinyl acetate)/multi-walled carbon nanotube nanocomposites. *Diamond Related Materials*. 2007; 16(4–7):1170–1173.
- [20] Verma SK, Bisarya SC. Improvement in properties of poly(vinyl acetate)-emulsion with dibasic acids. *Journal of Applied Polymer Science*. 1986; 31(8): 2675–2684.
- [21] Pekcan Ö, Evingür GA. Conductivity Percolation of Carbon Nanotubes in Polyacrylamide Gels. In: Siva Yellampalli, editor. *Carbon Nanotubes-Polymer Nanocomposites*. Croatia: InTech; 2011. 197 p. ISBN 978-953-307-498-6.
- [22] Evingür GA, Pekcan Ö. Drying of polyacrylamide-multiwalled carbon nanotube (MWNT) composites with various MWNTs contents: a fluorescence study. *Journal of Polymer Engineering*. 2013; 33(1): 33–39.
- [23] Evingür GA, Pekcan Ö. Monitoring of dynamical processes in PAAm-MWNTs composites by fluorescence method. *Advanced Composite Materials*. 2012; 21(2): 193–208.
- [24] Evingür GA, Pekcan Ö. Effect of multiwalled carbon nanotube (MWNT) on the behavior of swelling of polyacrylamide-MWNT composites. *Journal of Reinforced Plastics and Composites*. 2014; 33(13): 1196–1206.
- [25] Kara S, Pekcan Ö. Photon transmission technique for monitoring drying processes in acrylamide gels formed with various cross linker contents. *Journal of Applied Polymer Science*. 2001; 80(11): 1898–1906.
- [26] Birks JB. *Photophysics of aromatic molecules*. New York, NY: Wiley; 1971.
- [27] Tanaka T, Fillmore DJ. Kinetics of swelling of gels. *Journal Chemical Physics*. 1979; 70(3): 1214–1218.
- [28] Li Y, Tanaka T. Kinetics of swelling and shrinking of gels. *Journal Chemical Physics*. 1990; 92(2): 1365–1371.
- [29] Zrinyi M, Rosta J, Horkay F. Studies on the swelling and shrinking kinetics of chemically crosslinked disk-shaped poly(vinyl acetate) gels. *Macromolecules*. 1993; 26: 3097–3102.

- [30] Kara S, Arda E, Dolaştır F, Pekcan Ö. Electrical and optical percolations of polystyrene latex–multiwalled carbon nanotube composites. *Journal of Colloid and Interface Science*. 2010; 344: 395–401.
- [31] Arda E, Kara S, Pekcan Ö. Electrical, optical, and fluorescence percolations in P(VAc-co-BuA)/MWCNT composite films. *Phase Transitions*. 2013; 86(10): 1017–1032.
- [32] Stauffer D, Aharony A. *Introduction to Percolation Theory*. London: Taylor & Francis. 1994.
- [33] Ugur S, Yargı Ö, Pekcan Ö. Percolation and film formation behaviors of MWNT/PS nanocomposites. *Procedia Engineering*. 2011; 10: 1709–1717.
- [34] Yargı Ö, Ugur S, Pekcan Ö. Temperature dependence of oxygen diffusion into polymer/carbon nanotube. *Polymer Engineering & Science*. 2012; 52: 172–179.
- [35] Yargı Ö, Ugur S, Pekcan Ö. Oxygen diffusion into multiwalled carbon nanotube doped polystyrene latex films using fluorescence technique. *Journal of Fluorescence*. 2013; 23: 357–366.
- [36] Yargı Ö, Ugur S, Pekcan Ö. Fluorescence quenching method for monitoring oxygen diffusion into PS/CNT composite films. *Progress in Organic Coatings*. 2013; 76(12), 1805–1809.
- [37] Yargı Ö, Ugur S, Pekcan Ö. Polymer/carbon nanotube composite film formation: a fluorescence study. *Polymer Composites*. 2014; 35: 817–826.
- [38] Evingür GA, Pekcan Ö. Temperature effect on elasticity of swollen composite formed from polyacrylamide (PAAm)–multiwalled carbon nanotubes (MWNTs). *Engineering*. 2012; 4: 619–624.
- [39] Evingür GA, Pekcan Ö. Elastic percolation of polyacrylamide (PAAm)–multiwall carbon nanotubes (MWNTs) composites. *Phase Transition*. 2012; 85: 553–564.
- [40] Awasthi K, Awasthi S, Srivastava A, Kamalakaran R, Talapatra S, Ajayan PM, Srivastava ON. Synthesis and characterization of carbon nanotube–polyethylene oxide composites. *Nanotechnology*. 2006; 17: 5417–5422.
- [41] Du F, Scogna RC, Zhou W, Brand S, Fischer JE, Winey K. Nanotube networks in polymer nanocomposites: rheology and electrical conductivity. *Macromolecules*. 2004; 37: 9048–9055.
- [42] Pötschke P, Fornes TD, Paul DR. Rheological behavior of multiwalled carbonnanotube/polycarbonate composites. *Polymer*. 2002; 43: 3247–3255.
- [43] Meincke O, Kaempfer D, Weickmann H, Friedrich C, Vathauer M, Warth H. Mechanical properties and electrical conductivity of carbon–nanotube filled polyamide-6 and its blends with acrylonitrile/butadiene/styrene. *Polymer*. 2004; 45: 739–748
- [44] Sahimi M. *Application of Percolation Theory*. London: Taylor and Francis. 1994.

- [45] Weber M, Kamal MR. Estimation of the volume resistivity of electrically conductive composites. *Polymer Composites*. 1997; 18: 711–725.
- [46] Grunlan JC, Mehrabi AR, Bannon MV, Bahr JL. Water-based single-walled-nanotube-filled polymer composite with an exceptionally low percolation threshold. *Advanced Material*. 2004; 16: 150–152.

IntechOpen

IntechOpen

